Journal of Sound and Vibration 330 (2011) 162–181

Contents lists available at ScienceDirect

Journal of Sound and Vibration

journal homepage: www.elsevier.com/locate/jsvi

A 3D state-space solution for free-vibration analysis of a radially polarized laminated piezoelectric cylinder filled with fluid

W. Larbi, J.-F. Deü *

Conservatoire National des Arts et Métiers (Cnam), Structural Mechanics and Coupled Systems Laboratory, Chair of Mechanics, case 353, 2 rue Conté, 75003 Paris, France

ARTICLE INFO

Article history:
Received 14 December 2009
Received in revised form
9 July 2010
Accepted 2 August 2010
Handling Editor: A.V. Metrikine
Available online 9 September 2010

ABSTRACT

This paper presents a three-dimensional exact mixed state-space solution for the free-vibration analysis of simply-supported arbitrarily thick laminated piezoceramic hollow cylinders completely filled with fluid. The piezoelectric layers of the laminated cylinder are supposed to be polarized in the radial direction and the fluid is considered inviscid and compressible. This exact solution and the corresponding results can be used to develop accurate piezoelectric shell finite elements, and to investigate the effects of various parameters on the natural frequencies and mode shapes of the fluid/piezoelectric–structure coupled system.

1. Introduction

Theoretical modeling and simulation of smart structures is an active area of research since the early 1990s. Hence, for the purpose of verifying the accuracy of the widely used approximate theories or computational models of piezoelectric adaptive structures, the interest for exact analytical solutions has much increased during the last decade. These low-cost validation techniques are generally developed for static or free-vibration analyses of simply-supported structures. Most of the available literature on exact solutions for free vibration of smart structures has concerned piezoceramic plates. Thus, several three-dimensional (3D) exact [1–3] or approximate [4,5] and two-dimensional (2D) closed-form [6] solutions have been proposed in the literature for the free-vibration analysis of simply-supported (SS) piezoelectric laminated plates. Both through-the-thickness exponential distribution methods [1,4] and state-space approaches [2,5,7] have been used for the free-vibration problem formulation.

Many studies concerning analytical solutions of laminated piezoelectric cylinders have been proposed in the literature, including those described in the books of Parton and Kudryavtsev [8] and Tzou [9]. It is only recently that exact 3D solutions have been presented for the free-vibration analysis of simply-supported elastic [10,11] or piezoelectric [12,13] cylinder filled with fluid. Chen and Ding present [10] an exact solution for the free vibration of a simply supported, transversely isotropic cylindrical shell filled with compressible fluid. The displacement separation technique as well as the orthogonal series expansion method is employed in order to solve the problem. Bessel functions with complex arguments are directly used in the solution for the case of complex eigenvalues. Frequency equation of the coupled vibration problem is obtained by taking into account the effect of the inner fluid. The paper [11] describes a 3D exact solution of a simply supported arbitrarily thick hollow orthotropic cylinder completely filled with fluid. The formulation retains, as state variables, the standard mechanical displacements and transverses stresses for the structure augmented with the pressure

* Corresponding author. Tel.: +33 1 40272760; fax: +33 1 40272716.
E-mail address: jean-francois.deu@cnam.fr (J.-F. Deü).

0022-460X/$ - see front matter © 2010 Elsevier Ltd. All rights reserved.
doi:10.1016/j.jsv.2010.08.004

for the fluid. In [12], the coupled vibration of an inhomogeneous orthotropic piezoelectric hollow cylinder filled with internal compressible fluid is studied using the 3D equations of piezoelasticity. The cylinder is assumed to have a functionally graded property along the thickness direction (radial direction) and is polarized in the axial direction. A 3D exact solution of scattering and active acoustic control from a submerged piezoelectric-coupled orthotropic hollow cylinder is presented in [13]. The studied structure is an arbitrarily thick bilaminated circular hollow cylinder of infinite extent, which is composed of a cylindrically orthotropic axially polarized piezoelectric inner layer perfectly bonded to an orthotropic outer layer and filled with compressible fluid. The structure is excited by time-harmonic plane-progressive sound wave obliquely incident.

This paper presents a 3D exact mixed state-space solution, as well as a parametric analysis, for the free vibration of simply-supported arbitrarily thick laminated piezoceramic cylinder completely filled with fluid. The piezoelectric layers of the laminated cylinder are polarized in the radial direction. The fluid is inviscid and can be considered either compressible or incompressible. To the author's knowledge, this 3D solution, which is an extension of our conference paper [14], is detailed here for the first time. The proposed formulation, inspired by the one developed for the free-vibration analysis of laminated plates with embedded piezoceramic layers [7], retains, as state variables, the standard mechanical displacements and transverse stresses. These variables are augmented, for the piezoelectric case, by electric transverse displacement and potential, and for the fluid–structure coupled problem, by the fluid pressure. The classical transfer-matrix solution technique is employed to solve the problem. Natural frequencies and mode shapes are computed for different electrical boundary conditions at the inner and outer cylindrical surfaces of the piezoelectric layers. A parametric analysis is then conducted to show the influence of radius-to-thickness and length-to-thickness ratio, electric boundary conditions, and fluid effect. This exact solution and the corresponding results can be used to validate other analytical or numerical solutions.

2. Piezoelectric laminated state-space formulation

Consider a hollow circular cylinder of length L, internal radius R, having an arbitrarily constant thickness h and made of M orthotropic piezoelectric layers. The latter can have different thickness and material properties, but with material axes parallel to those of the adopted cylindrical coordinate system (e_r,e_θ,e_x) (see Fig. 1). The cylinder is mechanically unloaded while the piezoelectric layers are polarized along the radial axis and could be either charge-free (for open-circuited electrodes), or free of electric potential (for short-circuited electrodes).

The 3D linear constitutive equations of the jth piezoelectric layer, polarized along its material axis e_r, are for the converse and direct effects, respectively, given by

$$\begin{pmatrix}\sigma_{xx}\\ \sigma_{\theta\theta}\\ \sigma_{rr}\\ \sigma_{\theta r}\\ \sigma_{rx}\\ \sigma_{x\theta}\end{pmatrix}=\begin{pmatrix}c_{11}&c_{12}&c_{13}&0&0&0\\ c_{12}&c_{22}&c_{23}&0&0&0\\ c_{13}&c_{23}&c_{33}&0&0&0\\ 0&0&0&c_{44}&0&0\\ 0&0&0&0&c_{55}&0\\ 0&0&0&0&0&c_{66}\end{pmatrix}\begin{pmatrix}\varepsilon_{xx}\\ \varepsilon_{\theta\theta}\\ \varepsilon_{rr}\\ \gamma_{\theta r}\\ \gamma_{rx}\\ \gamma_{x\theta}\end{pmatrix}-\begin{pmatrix}0&0&e_{31}\\ 0&0&e_{32}\\ 0&0&e_{33}\\ 0&e_{24}&0\\ e_{15}&0&0\\ 0&0&0\end{pmatrix}\begin{pmatrix}E_x\\ E_\theta\\ E_r\end{pmatrix}$$

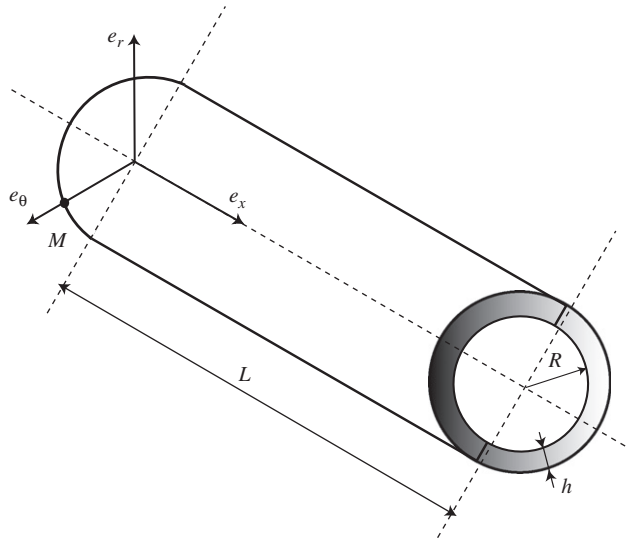

Fig. 1. Composite cylinder: geometry and notations.

and

$$\begin{pmatrix} d_x \\ d_\theta \\ d_r \end{pmatrix} = \begin{pmatrix} 0 & 0 & 0 & 0 & e_{15} & 0 \\ 0 & 0 & 0 & e_{24} & 0 & 0 \\ e_{31} & e_{32} & e_{33} & 0 & 0 & 0 \end{pmatrix} \begin{pmatrix} \varepsilon_{xx} \\ \varepsilon_{\theta\theta} \\ \varepsilon_{rr} \\ \gamma_{\theta r} \\ \gamma_{rx} \\ \gamma_{x\theta} \end{pmatrix} + \begin{pmatrix} \epsilon_{11} & 0 & 0 \\ 0 & \epsilon_{22} & 0 \\ 0 & 0 & \epsilon_{33} \end{pmatrix} \begin{pmatrix} E_x \\ E_\theta \\ E_r \end{pmatrix}$$

where σ_{ij} and d_i $(i,j=x,\theta,r)$ are the stress tensor and the electric displacement vector components; c_{IJ}, e_{kJ} and ϵ_{kl} $(k,l=1,2,3;$ $I,J=1,\ldots,6)$ denote elastic, piezoelectric and dielectric material constants.

The strain tensor ε_{ij} (and γ_{ij}) and electric field vector E_i components are linked to the mechanical displacement u_i and electric potential ϕ by the usual gradient relations

$$\varepsilon_{xx} = \frac{\partial u_x}{\partial x}, \quad \varepsilon_{\theta\theta} = \frac{1}{r}\frac{\partial u_\theta}{\partial \theta} + \frac{u_r}{r}, \quad \varepsilon_{rr} = \frac{\partial u_r}{\partial r}$$

$$\gamma_{\theta r} = \frac{1}{r}\frac{\partial u_r}{\partial \theta} + \frac{\partial u_\theta}{\partial r} - \frac{u_\theta}{r}, \quad \gamma_{rx} = \frac{\partial u_r}{\partial x} + \frac{\partial u_x}{\partial r}, \quad \gamma_{x\theta} = \frac{1}{r}\frac{\partial u_x}{\partial \theta} + \frac{\partial u_\theta}{\partial x}$$

$$E_x = -\frac{\partial \phi}{\partial x}, \quad E_\theta = -\frac{\partial \phi}{r\partial \theta}, \quad E_r = -\frac{\partial \phi}{\partial r}$$

Substituting the latter in the constitutive equations, then combining some of the resulting equations provides the radial derivatives of the mechanical displacements and electric potential

$$\frac{\partial u_x}{\partial r} = -\frac{\partial u_r}{\partial x} - \frac{e_{15}}{c_{55}}\frac{\partial \phi}{\partial x} + \frac{\sigma_{rx}}{c_{55}} \tag{1a}$$

$$\frac{\partial u_\theta}{\partial r} = \frac{u_\theta}{r} - \frac{1}{r}\frac{\partial u_r}{\partial \theta} - \frac{1}{r}\frac{e_{24}}{c_{44}}\frac{\partial \phi}{\partial \theta} + \frac{\sigma_{\theta r}}{c_{44}} \tag{1b}$$

$$\frac{\partial u_r}{\partial r} = -\frac{\alpha_{13}}{\alpha_{33}}\frac{\partial u_x}{\partial x} - \frac{1}{r}\frac{\alpha_{23}}{\alpha_{33}}\frac{\partial u_\theta}{\partial \theta} - \frac{\alpha_{23}}{\alpha_{33}}\frac{u_r}{r} + \frac{\epsilon_{33}}{\alpha_{33}}\sigma_{rr} + \frac{e_{33}}{\alpha_{33}}d_r \tag{1c}$$

$$\frac{\partial \phi}{\partial r} = -\frac{\beta_{13}}{\alpha_{33}}\frac{\partial u_x}{\partial x} - \frac{1}{r}\frac{\beta_{23}}{\alpha_{33}}\frac{\partial u_\theta}{\partial \theta} - \frac{\beta_{23}}{\alpha_{33}}\frac{u_r}{r} + \frac{e_{33}}{\alpha_{33}}\sigma_{rr} - \frac{c_{33}}{\alpha_{33}}d_r \tag{1d}$$

with the following constants:

$$\alpha_{13} = c_{13}\epsilon_{33} + e_{33}e_{31}, \quad \alpha_{23} = c_{23}\epsilon_{33} + e_{33}e_{32}, \quad \alpha_{33} = c_{33}\epsilon_{33} + e_{33}^2$$

$$\beta_{13} = c_{13}e_{33} - c_{33}e_{31}, \quad \beta_{23} = c_{23}e_{33} - c_{33}e_{32}$$

The electrodynamics response of the jth piezoelectric lamina, free of mechanical and electric body loads, is governed by the classical stress and charge equations, respectively,

$$\frac{\partial \sigma_{xx}}{\partial x} + \frac{1}{r}\frac{\partial \sigma_{x\theta}}{\partial \theta} + \frac{\partial \sigma_{rx}}{\partial r} + \frac{\sigma_{rx}}{r} = \rho_S \frac{\partial^2 u_x}{\partial t^2}$$

$$\frac{\partial \sigma_{x\theta}}{\partial x} + \frac{1}{r}\frac{\partial \sigma_{\theta\theta}}{\partial \theta} + \frac{\partial \sigma_{\theta r}}{\partial r} + \frac{2\sigma_{\theta r}}{r} = \rho_S \frac{\partial^2 u_\theta}{\partial t^2}$$

$$\frac{\partial \sigma_{rx}}{\partial x} + \frac{1}{r}\frac{\partial \sigma_{\theta r}}{\partial \theta} + \frac{\partial \sigma_{rr}}{\partial r} + \frac{\sigma_{rr} - \sigma_{\theta\theta}}{r} = \rho_S \frac{\partial^2 u_r}{\partial t^2}$$

and

$$\frac{\partial d_x}{\partial x} + \frac{1}{r}\frac{\partial d_\theta}{\partial \theta} + \frac{\partial d_r}{\partial r} + \frac{d_r}{r} = 0$$

where ρ_S is the mass density of the cylinder.

After combining some of the previous equations, the thickness first derivatives of the radial stresses and radial electric displacement can be written as

$$\frac{\partial \sigma_{rr}}{\partial r} = \frac{c_{12}^*}{r}\frac{\partial u_x}{\partial x} + \frac{c_{22}^*}{r^2}\frac{\partial u_\theta}{\partial \theta} + \rho_S \frac{\partial^2 u_r}{\partial t^2} + \frac{c_{22}^*}{r^2}u_r + \frac{\alpha_{23} - \alpha_{33}}{\alpha_{33}}\frac{\sigma_{rr}}{r} - \frac{1}{r}\frac{\partial \sigma_{\theta r}}{\partial \theta} - \frac{\partial \sigma_{rx}}{\partial x} + \frac{\beta_{23}}{\alpha_{33}}\frac{d_r}{r} \tag{2a}$$

$$\frac{\partial \sigma_{rx}}{\partial r} = \rho_S \frac{\partial^2 u_x}{\partial t^2} - c_{11}^* \frac{\partial^2 u_x}{\partial x^2} - \frac{c_{66}}{r^2}\frac{\partial u_x^2}{\partial \theta^2} - \frac{c_{12}^* + c_{66}}{r}\frac{\partial^2 u_\theta}{\partial x \partial \theta} - \frac{c_{12}^*}{r}\frac{\partial u_r}{\partial x} - \frac{\alpha_{13}}{\alpha_{33}}\frac{\partial \sigma_{rr}}{\partial x} - \frac{\sigma_{rx}}{r} - \frac{\beta_{13}}{\alpha_{33}}\frac{\partial d_r}{\partial x} \tag{2b}$$

$$\frac{\partial \sigma_{\theta r}}{\partial r} = -\frac{c_{12}^{*}+c_{66}}{r}\frac{\partial^2 u_x}{\partial \theta \partial x} + \rho_S \frac{\partial^2 u_\theta}{\partial t^2} - c_{66}\frac{\partial^2 u_\theta}{\partial x^2} - \frac{c_{22}^{*}}{r^2}\frac{\partial^2 u_\theta}{\partial \theta^2} - \frac{c_{22}^{*}}{r^2}\frac{\partial u_r}{\partial \theta} - \frac{\alpha_{23}}{\alpha_{33}}\frac{1}{r}\frac{\partial \sigma_{rr}}{\partial \theta} - \frac{2\sigma_{\theta r}}{r} - \frac{\beta_{23}}{\alpha_{33}}\frac{1}{r}\frac{\partial d_r}{\partial \theta} \tag{2c}$$

$$\frac{\partial d_r}{\partial r} = -\frac{e_{24}}{c_{44}}\frac{1}{r}\frac{\partial \sigma_{\theta r}}{\partial \theta} - \frac{e_{15}}{c_{55}}\frac{\sigma_{rx}}{\partial x} + \epsilon_{11}^{*}\frac{\partial^2 \phi}{\partial x^2} + \frac{\epsilon_{22}^{*}}{r^2}\frac{\partial^2 \phi}{\partial \theta^2} - \frac{d_r}{r} \tag{2d}$$

with the following constants:

$$c_{11}^{*} = c_{11} - (c_{13}\alpha_{13} + e_{31}\beta_{13})/\alpha_{33}\ , \quad c_{22}^{*} = c_{22} - (c_{23}\alpha_{23} + e_{32}\beta_{23})/\alpha_{33}$$

$$c_{12}^{*} = c_{12} - (c_{13}\alpha_{23} + e_{31}\beta_{23})/\alpha_{33} = c_{12} - (c_{23}\alpha_{13} + e_{32}\beta_{13})/\alpha_{33}$$

$$\epsilon_{11}^{*} = \epsilon_{11} + e_{15}^2/c_{55}, \quad \epsilon_{22}^{*} = \epsilon_{22} + e_{24}^2/c_{44}$$

The combination of Eqs. (1) and (2) gives the jth piezoelectric lamina state-space equation

$$\frac{\partial}{\partial \overline{r}}\begin{pmatrix}\mathbf{x}_1\\ \mathbf{x}_2\end{pmatrix} = \begin{pmatrix}\mathbf{a}_{11} & \mathbf{a}_{12}\\ \mathbf{a}_{21} & \mathbf{a}_{22}\end{pmatrix}\begin{pmatrix}\mathbf{x}_1\\ \mathbf{x}_2\end{pmatrix} \tag{3}$$

where

$$\mathbf{x}_1 = (u_x\ \ u_\theta\ \ \sigma_{rr}\ \ d_r)^{\mathrm{T}}, \quad \mathbf{x}_2 = (\sigma_{rx}\ \ \sigma_{\theta r}\ \ u_r\ \ \phi)^{\mathrm{T}}$$

The matrices $\mathbf{a}_{ij}$ (i,j=1,2) are given in Appendix A. It can be seen that the sub-matrices $\mathbf{a}_{12}$ and $\mathbf{a}_{21}$ are individually symmetric thanks to the chosen order of the components of the state sub-vectors $\mathbf{x}_1$ and $\mathbf{x}_2$ but the system matrix of Eq. (3) remains not symmetric.

3. Simply-supported piezoelectric cylinder

We now consider the free vibrations of a hollow cylinder subjected to simply-supported mechanical boundary conditions and short-circuited electrical conditions at x=0 and L. These conditions can be written as

$$u_r = u_\theta = \sigma_{xx} = \phi = 0 \quad \text{at } x = 0, L \tag{4}$$

The mixed state variables that satisfy the previous electromechanical boundary conditions can be written in trigonometric series as

$$\begin{pmatrix}u_x\\ u_\theta\\ \sigma_{rr}\\ d_r\\ \sigma_{rx}\\ \sigma_{\theta r}\\ u_r\\ \phi\end{pmatrix} = \sum_{m=0}^{\infty}\sum_{n=0}^{\infty}\begin{pmatrix} RU_x(\overline{r})\ \cos m\pi\overline{x}\ \cos n\theta\\ RU_\theta(\overline{r})\ \sin m\pi\overline{x}\ \sin n\theta\\ c_{66}^1\Sigma_{rr}(\overline{r})\ \sin m\pi\overline{x}\ \cos n\theta\\ \sqrt{c_{66}^1\epsilon_{33}^1}D_r(\overline{r})\ \sin m\pi\overline{x}\ \cos n\theta\\ c_{66}^1\Sigma_{rx}(\overline{r})\ \cos m\pi\overline{x}\ \cos n\theta\\ c_{66}^1\Sigma_{\theta r}(\overline{r})\ \sin m\pi\overline{x}\ \sin n\theta\\ RU_r(\overline{r})\ \sin m\pi\overline{x}\ \cos n\theta\\ R\sqrt{c_{66}^1/\epsilon_{33}^1}\Phi(\overline{r})\ \sin m\pi\overline{x}\ \cos n\theta\end{pmatrix}\exp \mathrm{i}\omega t \tag{5}$$

where ω is the circular frequency (rad/s); i is the imaginary unit ($\mathrm{i}^2 = -1$); $\overline{r} = r/R$ and $\overline{x} = x/L$; the superscript 1 indicates a quantity in the first layer of the cylinder; m and n are the half-wavenumbers in the axial and circumferential directions, respectively. Moreover, the uppercase letters denote the non-dimensional amplitudes of the corresponding lowercase physical quantities.

It is worthwhile to notice that Fourier series of Eqs. (5) is summed on m and n. However, in the free-vibration analysis, it is well known that due to the orthogonal trigonometric functions, these summations uncouple and the corresponding eigenvalue problem can be solved for each (m,n) couple.

The substitution of Eqs. (5) in the state-space equation (3), transforms it into

$$\frac{\partial}{\partial \overline{\overline{r}}}\begin{pmatrix}\mathbf{X}_1\\ \mathbf{X}_2\end{pmatrix} = \begin{pmatrix}\mathbf{A}_{11} & \mathbf{A}_{12}\\ \mathbf{A}_{21} & \mathbf{A}_{22}\end{pmatrix}\begin{pmatrix}\mathbf{X}_1\\ \mathbf{X}_2\end{pmatrix} \tag{6}$$

where

$$\mathbf{X}_1 = (U_x\ \ U_\theta\ \ \Sigma_{rr}\ \ D_r)^{\mathrm{T}}, \quad \mathbf{X}_2 = (\Sigma_{rx}\ \ \Sigma_{\theta r}\ \ -U_r\ \ -\Phi)^{\mathrm{T}}$$

and

$$\mathbf{A}_{11}=\left(\begin{array}{c|c|c|c} 0 & 0 & 0 & 0 \\ \hline 0 & \frac{1}{\bar{r}} & 0 & 0 \\ \hline -\frac{c_{12}^{*}}{c_{66}^{1}}\frac{\lambda}{\bar{r}} & \frac{c_{22}^{*}}{c_{66}^{1}}\frac{n}{\bar{r}^2} & \frac{\alpha_{23}-\alpha_{33}}{\alpha_{33}}\frac{1}{\bar{r}} & \frac{\beta_{23}}{\alpha_{33}}\sqrt{\frac{\epsilon_{33}^{1}}{c_{66}^{1}}}\frac{1}{\bar{r}} \\ \hline 0 & 0 & 0 & -\frac{1}{\bar{r}} \end{array}\right)$$

$$\mathbf{A}_{12}=\left(\begin{array}{c|c|c|c} \frac{c_{66}^{1}}{c_{55}} & 0 & \lambda & \frac{e_{15}}{c_{55}}\sqrt{\frac{c_{66}^{1}}{\epsilon_{33}^{1}}}\lambda \\ \hline 0 & \frac{c_{66}^{1}}{c_{44}} & -\frac{n}{\bar{r}} & -\frac{e_{24}}{c_{44}}\sqrt{\frac{c_{66}^{1}}{\epsilon_{33}^{1}}}\frac{n}{\bar{r}} \\ \hline \lambda & -\frac{n}{\bar{r}} & \frac{\rho_S}{\rho_S^{1}}\bar{\omega}^2-\frac{c_{22}^{*}}{c_{66}^{1}}\frac{1}{\bar{r}^2} & 0 \\ \hline \frac{e_{15}}{c_{55}}\sqrt{\frac{c_{66}^{1}}{\epsilon_{33}^{1}}}\lambda & -\frac{e_{24}}{c_{44}}\sqrt{\frac{c_{66}^{1}}{\epsilon_{33}^{1}}}\frac{n}{\bar{r}} & 0 & \frac{\epsilon_{11}^{*}}{\epsilon_{33}^{1}}\lambda^2+\frac{\epsilon_{22}^{*}}{\epsilon_{33}^{1}}\frac{n^2}{\bar{r}^2} \end{array}\right)$$

$$\mathbf{A}_{21}=\left(\begin{array}{c|c|c|c} -\frac{\rho_S}{\rho_S^{1}}\bar{\omega}^2+\frac{c_{11}^{*}}{c_{66}^{1}}\lambda^2+\frac{c_{66}}{c_{66}^{1}}\frac{n^2}{\bar{r}^2} & -\frac{c_{12}^{*}+c_{66}}{c_{66}^{1}}\frac{n\lambda}{\bar{r}} & -\frac{\alpha_{13}}{\alpha_{33}}\lambda & -\frac{\beta_{13}}{\alpha_{33}}\sqrt{\frac{\epsilon_{33}^{1}}{c_{66}^{1}}}\lambda \\ \hline -\frac{c_{12}^{*}+c_{66}}{c_{66}^{1}}\frac{n\lambda}{\bar{r}} & -\frac{\rho_S}{\rho_S^{1}}\bar{\omega}^2+\frac{c_{66}}{c_{66}^{1}}\lambda^2+\frac{c_{22}^{*}}{c_{66}^{1}}\frac{n^2}{\bar{r}^2} & \frac{\alpha_{23}}{\alpha_{33}}\frac{n}{\bar{r}} & \frac{\beta_{23}}{\alpha_{33}}\sqrt{\frac{\epsilon_{33}^{1}}{c_{66}^{1}}}\frac{n}{\bar{r}} \\ \hline -\frac{\alpha_{13}}{\alpha_{33}}\lambda & \frac{\alpha_{23}}{\alpha_{33}}\frac{n}{\bar{r}} & -\frac{c_{66}^{1}\epsilon_{33}}{\alpha_{33}} & -\frac{e_{33}\sqrt{c_{66}^{1}\epsilon_{33}^{1}}}{\alpha_{33}} \\ \hline -\frac{\beta_{13}}{\alpha_{33}}\sqrt{\frac{\epsilon_{33}^{1}}{c_{66}^{1}}}\lambda & \frac{\beta_{23}}{\alpha_{33}}\sqrt{\frac{\epsilon_{33}^{1}}{c_{66}^{1}}}\frac{n}{\bar{r}} & -\frac{e_{33}\sqrt{c_{66}^{1}\epsilon_{33}^{1}}}{\alpha_{33}} & \frac{c_{33}\epsilon_{33}^{1}}{\alpha_{33}} \end{array}\right)$$

$$\mathbf{A}_{22}=\left(\begin{array}{c|c|c|c} -\frac{1}{\bar{r}} & 0 & \frac{c_{12}^{*}}{c_{66}^{1}}\frac{\lambda}{\bar{r}} & 0 \\ \hline 0 & -\frac{2}{\bar{r}} & -\frac{c_{22}^{*}}{c_{66}^{1}}\frac{n}{\bar{r}^2} & 0 \\ \hline 0 & 0 & -\frac{\alpha_{23}}{\alpha_{33}}\frac{1}{\bar{r}} & 0 \\ \hline 0 & 0 & -\frac{\beta_{23}}{\alpha_{33}}\sqrt{\frac{\epsilon_{33}^{1}}{c_{66}^{1}}}\frac{1}{\bar{r}} & 0 \end{array}\right)$$

with

$$\lambda=m\pi R/L,\quad \bar{\omega}=\omega R\sqrt{\rho_S^{1}/c_{66}^{1}}.$$

It is important to note that the previous matrices, which are associated to the jth piezoelectric lamina, are not constant (some terms depend on $\bar{r}$) making difficult the resolution of Eq. (6). In the resolution method, which will be explained in Section 6, each layer of the laminated cylinder is divided into thin sub-layers such that the previous matrices can be assumed constant within each sub-layer. It can also be noted that the matrices $\mathbf{A}_{12}$ and $\mathbf{A}_{21}$ become symmetric by choosing $-U_r$ and $-\Phi$ instead of U_r and Φ, respectively, in $\mathbf{X}_2$.

4. Compressible fluid motion

We consider in this section a homogeneous, inviscid and compressible fluid, gravity effects being neglected. The pressure field p in the fluid is then governed by the wave equation

$$\Delta p-\frac{1}{c_F^2}\frac{\partial^2 p}{\partial t^2}=0 \tag{7}$$

where c_F is the constant speed of sound in the fluid. In the cylindrical polar coordinate system, this equation is written in the following form:

$$\frac{\partial^2 p}{\partial x^2}+\frac{1}{r^2}\frac{\partial^2 p}{\partial \theta^2}+\frac{\partial^2 p}{\partial r^2}+\frac{1}{r}\frac{\partial p}{\partial r}-\frac{1}{c_F^2}\frac{\partial^2 p}{\partial t^2}=0 \tag{8}$$

As for the structure variables, fluid pressure can be expressed in terms of trigonometric series by

$$p=\rho_F c_F^2\sum_{m=0}^{\infty}\sum_{n=0}^{\infty}P(\bar{r})\sin m\pi\bar{x}\cos n\theta\exp \mathrm{i}\omega t \tag{9}$$

where ρ_F is the mass density of the fluid. Note that the choice of the sine and cosine functions in Eq. (9) is link to the continuity conditions at the fluid–structure interface.

The substitution of Eq. (9) in Eq. (8) leads to

$$\bar{r}^2\frac{\partial^2 P}{\partial \bar{r}^2}+\bar{r}\frac{\partial P}{\partial \bar{r}}+(\nu^2\bar{r}^2-n^2)P=0 \tag{10}$$

where $\nu^2=\omega^2R^2/c_F^2-\lambda^2$.

Eq. (10) represents a Bessel equation whose solution depends on the sign of ν^2:

- for $\nu^2>0$:

$$P=AJ_n(\nu\bar{r})+BY_n(\nu\bar{r})\Rightarrow\frac{\partial P}{\partial \bar{r}}=A\nu J_n'(\nu\bar{r})+B\nu Y_n'(\nu\bar{r}) \tag{11}$$

  where J_n and Y_n represents, respectively, Bessel function and modified Bessel function of the first kind and order n. Moreover, A and B are constants obtained from the boundary conditions.
- for $\nu^2=0$ and $n\neq 0$:

$$P=E\bar{r}^n\Rightarrow\frac{\partial P}{\partial \bar{r}}=nE\bar{r}^{n-1} \tag{12}$$

  where E is the constant obtained from the boundary conditions.
- for $\nu^2=0$ and $n=0$:

$$P=F\ln(\bar{r})\Rightarrow\frac{\partial P}{\partial \bar{r}}=\frac{F}{\bar{r}} \tag{13}$$

  where F is the constant obtained from the boundary conditions.
- for $\nu^2=-w^2<0$:

$$P=CI_n(w\bar{r})+DK_n(w\bar{r})\Rightarrow\frac{\partial P}{\partial \bar{r}}=CwI_n'(w\bar{r})+DwK_n'(w\bar{r}) \tag{14}$$

  where I_n and K_n represents, respectively, modified Bessel function of the first and second kind, respectively. Moreover, C and D are constants obtained from the boundary conditions.

5. Boundary conditions at the fluid–structure interface

We consider now that the simply-supported cylindrical cavity is completely filled with fluid. At the fluid–structure interface ($\bar{r}=1$), we have the continuity conditions of the radial displacement (deduced from the linearized Euler equation) and the normal stress. These two conditions lead to

$$p=-\sigma_{rr}\quad\text{for } r=R\Rightarrow P=-\frac{c_{66}}{\rho_F c_F^2}\Sigma_{rr}\quad\text{for }\bar{r}=1 \tag{15a}$$

$$\frac{\partial p}{\partial r}=-\rho_F\frac{\partial^2 u_r}{\partial t^2}\quad\text{for } r=R\Rightarrow\frac{\partial P}{\partial \bar{r}}=\omega^2\frac{R^2}{c_F^2}U_r\quad\text{for }\bar{r}=1 \tag{15b}$$

The third boundary condition is obtained on the axis of the cylinder ($\bar{r}=0$) due to the axisymmetry of the problem. This condition is written as

$$\frac{\partial p}{\partial r}=0\quad\text{for } r=0\Rightarrow\frac{\partial P}{\partial \bar{r}}=0\quad\text{for }\bar{r}=0 \tag{16}$$

Using Eq. (16), $P(\overline{r})$ can be reduced to

$$P(\overline{r}) = \begin{cases} AJ_n(\nu\overline{r}) & \text{for} \quad \nu^2 > 0 \\ E\overline{r}^n & \text{for} \quad \nu^2 = 0 \ \text{ and } \ n \neq 0 \\ F\ln(\overline{r}) & \text{for} \quad \nu^2 = 0 \ \text{ and } \ n = 0 \\ CI_n(w\overline{r}) & \text{for} \quad \nu^2 = -w^2 < 0 \end{cases} \tag{17}$$

which gives the derivatives of $P(\overline{r})$:

$$\frac{\partial P(\overline{r})}{\partial \overline{r}} = \begin{cases} A\nu J_n'(\nu\overline{r}) & \text{for} \quad \nu^2 > 0 \\ En\overline{r}^{n-1} & \text{for} \quad \nu^2 = 0 \ \text{ and } \ n \neq 0 \\ \dfrac{F}{\overline{r}} & \text{for} \quad \nu^2 = 0 \ \text{ and } \ n = 0 \\ CwI_n'(w\overline{r}) & \text{for} \quad \nu^2 = -w^2 < 0 \end{cases} \tag{18}$$

Using Eqs. (18) and the continuity condition of the radial displacement at the interface $\overline{r} = 1$ (Eq. (15b)), the constants A, E, F and C are given by

$$\begin{cases} A = \dfrac{\omega^2 R^2}{c_F^2 \nu J_n'(\nu)} U_r(1) & \text{for} \quad \nu^2 > 0 \\ E = \dfrac{\omega^2 R^2}{n c_F^2} U_r(1) & \text{for} \quad \nu^2 = 0 \ \text{ and } \ n \neq 0 \\ F = \dfrac{\omega^2 R^2}{c_F^2} U_r(1) & \text{for} \quad \nu^2 = 0 \ \text{ and } \ n = 0 \\ C = \dfrac{\omega^2 R^2}{c_F^2 w I_n'(w)} U_r(1) & \text{for} \quad \nu^2 = -w^2 < 0 \end{cases} \tag{19}$$

Finally, using the continuity condition of the normal stress at the interface $\overline{r} = 1$ (Eq. (15a)) and replacing P by its expression (17), the radial stress at the fluid–structure interface can be obtained for any value of ν^2

$$\Sigma_{rr}(1) = -\frac{\rho_F}{\rho_S}\overline{\omega}^2 U_r(1) Q(1) \tag{20}$$

where $Q(1)$ is the value at the fluid–structure interface of the following function:

$$Q(1) = \begin{cases} \dfrac{J_n(\nu)}{J_n'(\nu)}\dfrac{1}{\nu} = \dfrac{J_n(\nu)}{J_{n-1}(\nu) - J_{n+1}(\nu)}\dfrac{2}{\nu} & \text{for } \nu^2 > 0 \\ \dfrac{1}{n} & \text{for } \nu^2 = 0 \ \text{ and } \ n \neq 0 \\ 0 & \text{for } \nu^2 = 0 \ \text{ and } \ n = 0 \\ \dfrac{I_n(w)}{I_n'(w)}\dfrac{1}{w} = \dfrac{I_n(w)}{I_{n-1}(w) + I_{n+1}(w)}\dfrac{2}{w} & \text{for } \nu^2 = -w^2 < 0 \end{cases}$$

The radial stress at the fluid–structure interface given in Eq. (20) will be used as boundary condition in the free vibration problem described below.

6. Resolution of the free-vibration problem

As previously mentioned, for the resolution of the free-vibration problem, the laminated cylinder must be decomposed into N thin sub-layers (see Fig. 2).

For each sub-layer k, Eq. (6) can be written in condensed form

$$\frac{\partial}{\partial \overline{r}}\mathbf{X}^{(k)} = \mathbf{A}_k \mathbf{X}^{(k)} \tag{21}$$

where $\mathbf{A}_k$ is now a constant matrix computed at the average radius of the sub-layer k. The solution of Eq. (21) can then be written in the following transfer matrix form:

$$\mathbf{X}^{(k)}(\overline{r}_{k+1}) = \mathbf{T}_k \mathbf{X}^{(k)}(\overline{r}_k) \tag{22}$$

with

$$\mathbf{T}_k = \exp(h_k \mathbf{A}_k)$$

where h_k is the thickness of the kth sub-layer and $\mathbf{T}_k$ its lamina transfer matrix which maps the state vector at its bottom surface to that at its top.

The eigenvalue problem to be solved for the free-vibration analysis is obtained by the assembly of the sub-layer transfer matrices using the appropriate interface continuity conditions.

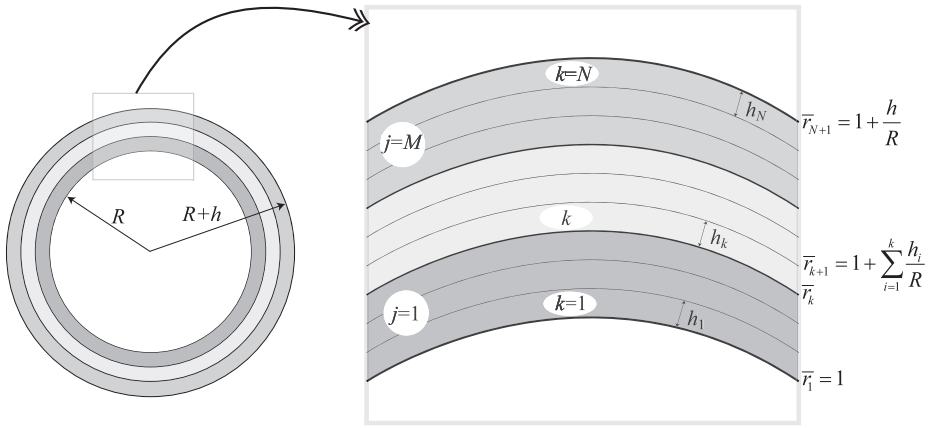

Fig. 2. Through-thickness view of the laminated composite cylinder.

Classically, the mechanical displacements and radial stresses, as well as electric radial displacement and potential are considered continuous across the interface between k and $k+1$ sub-layers. Hence, the electromechanical interface continuity relations can be written in terms of the full state vector by

$$\mathbf{X}^{(k+1)}(\overline{r}_{k+1}) = \mathbf{X}^{(k)}(\overline{r}_{k+1}) \tag{23}$$

for $k=1,\ldots,N-1$.

Using recursively Eq. (23), combined with Eqs. (22), provides an eighth-order assembled transfer matrix equation

$$\mathbf{X}|_{\overline{r}=1+h/R} = \mathbf{T}\mathbf{X}|_{\overline{r}=1} \tag{24}$$

where the transfer matrix is the product of the sub-layer transfer matrices

$$\mathbf{T} = \prod_{k=N}^{1} \mathbf{T}_k$$

After suitable rows and columns interchanges, Eq. (24) can be written as

$$\begin{pmatrix} \mathbf{X}_U \\ \mathbf{X}_\Sigma \end{pmatrix}_{\overline{r}=1+h/R} = \begin{pmatrix} \mathbf{T}_{UU} & \mathbf{T}_{U\Sigma} \\ \mathbf{T}_{\Sigma U} & \mathbf{T}_{\Sigma\Sigma} \end{pmatrix} \begin{pmatrix} \mathbf{X}_U \\ \mathbf{X}_\Sigma \end{pmatrix}_{\overline{r}=1} \tag{25}$$

where the vectors $\mathbf{X}_U$ and $\mathbf{X}_\Sigma$ are given by

- in open-circuited (OC) configuration:

$$\mathbf{X}_U = (U_x \;\; U_\theta \;\; -U_r \;\; -\Phi)^{\mathrm{T}}, \quad \mathbf{X}_\Sigma = (\Sigma_{rr} \;\; \Sigma_{rx} \;\; \Sigma_{r\theta} \;\; D_r)^{\mathrm{T}} \tag{26}$$

- in short-circuited (SC) configuration:

$$\mathbf{X}_U = (U_x \;\; U_\theta \;\; -U_r \;\; D_r)^{\mathrm{T}}, \quad \mathbf{X}_\Sigma = (\Sigma_{rr} \;\; \Sigma_{rx} \;\; \Sigma_{r\theta} \;\; -\Phi)^{\mathrm{T}} \tag{27}$$

The external surface of the cylinder is free of transverse stresses and can be either free of electric radial displacement (in OC configuration) or free of electric potential (in SC configuration) such that $\mathbf{X}_\Sigma(1+h/R) = \mathbf{0}$. At the inner surface, we have $\Sigma_{rx}(1) = \Sigma_{r\theta}(1) = 0$ and either $D_r(1)=0$ (in OC configuration) or $\Phi(1) = 0$ (in SC configuration). Moreover, due to the internal fluid, $\Sigma_{rr}(1)$ satisfies Eq. (20). Considering all these boundary conditions, Eq. (25) gives

$$\mathbf{0} = \overline{\mathbf{T}}_{\Sigma U}\mathbf{X}_U(1) \tag{28}$$

where

$$\overline{\mathbf{T}}_{\Sigma U} = \mathbf{T}_{\Sigma U} + \overline{\omega}^2 U_r(1)Q(1)\begin{pmatrix} \mathbf{T}_{\Sigma\Sigma}(1,1) & 0 & 0 & 0 \\ \mathbf{T}_{\Sigma\Sigma}(2,1) & 0 & 0 & 0 \\ \mathbf{T}_{\Sigma\Sigma}(3,1) & 0 & 0 & 0 \\ \mathbf{T}_{\Sigma\Sigma}(4,1) & 0 & 0 & 0 \end{pmatrix}$$

For non-trivial solution of Eq. (28), the determinant of the matrix $\overline{\mathbf{T}}_{\Sigma U}$ must vanish. Thus, the natural frequencies of the composite piezoelectric cylinder filled with a compressible fluid can be obtained by solving the following equation:

$$\det\overline{\mathbf{T}}_{\Sigma U} = 0 \tag{29}$$

This equation is solved numerically using Matlab software for several values of $\overline{\omega}$ in a given frequency range. Once a change of sign is found for the determinant, the bisection method is used to refine the root estimation to the required

accuracy. It can be notice that, for fixed (m,n) couple, an infinite number of solutions exist for Eq. (29), representing the so-called thickness modes (denoted t). For each calculated natural frequency, identified by the (m,n,t) triplet, the initial state vector $\mathbf{X}_U(1)$ is next computed using Eq. (28). Then, the interface unknowns are deduced from Eq. (22) for a given electric boundary conditions. After that, the through-the-thickness distributions of the electromechanical variables can be evaluated.

7. Numerical examples

7.1. Laminated composite cylinder filled with fluid

We consider in this first example a three-layer cross-ply $[0^\circ,90^\circ,0^\circ]$ simply-supported cylinder filled with a compressible fluid. The material and geometric data of the cylinder are given in Table 1 and the fluid is characterized by a mass density $\rho_F = 1000\,\mathrm{kg/m^3}$ and a speed of sound c_F=1500 m/s.

Table 2 shows a comparison of the frequency parameter $\omega^\star = \omega R\sqrt{\rho_S/E_2}$ for the empty shell computed by our method and those given in [15] using an analytical solution based on Love's shell theory, and in [16] using the wave propagation method. An excellent agreement can be observed for all modes, thus validating the state-space method for laminated elastic structures. It can also be noted that for shells with small length-to-radius ratios, as in the case L/R=1, the minimum frequency occurs for the larger n. Nevertheless, for L/R=10, the natural frequencies decrease when n varies from 1 to 4, and increase for n larger than 4.

Table 3 presents the frequencies of the fluid–structure coupled system given by the proposed exact solution and those obtained by the finite element method developed by the authors in [17]. We recall that the shell finite element is based on the Kirchhoff–Love theory. The results, given for the six first circumferential harmonics, show a good agreement between the two methods. This free-vibration example validate the numerical implementation of the previously described state-space solution in a fluid–structure case.

7.2. Free vibration of a piezoelectric cylindrical shell filled with a compressible fluid

In order to validate and analyze the formulation for piezoelectric materials, we present in this example a comparative study for a simply-supported single-layer piezoelectric cylindrical shell with or without internal compressible fluid. The geometrical properties are L=30 mm, R=4.5 mm and h=0.5 mm. Moreover, the piezoelectric material is the PZT-5H (see Table 7 for the properties) and the considered fluid has a mass density $\rho_F = 1000\,\mathrm{kg/m^3}$ and a speed of sound c_F=1500 m/s. Note that a null pressure is prescribed at both ends of the fluid cylinder.

The differences between SC and OC natural frequencies are used to evaluate the effective modal coupling coefficient EMCC [18] which represents physically the percentage of the mechanical strain energy converted into the electric one and vice versa,

$$\mathrm{EMCC}\ (\%) = 100 \times \sqrt{\frac{\omega_{OC}^2 - \omega_{SC}^2}{\omega_{OC}^2}} \tag{30}$$

The first 20 modes of the piezoelectric cylinder were computed using the proposed exact solution for (i) elastic case, (ii) short-circuited case ($\phi = 0$) and (iii) open-circuited case (D=0). Elastic modes have been also calculated with the finite element code MSC-Nastran to check the modes identification.

For illustration purpose, the roots of the characteristic equation (29) are presented in Fig. 3 in the elastic case for n=1 and m=1.

The obtained results are shown in Table 4 for the non-dimensional frequencies and EMCC, and in Fig. 4 for the first 10 modal shapes. They indicate that:

- The elastic results are in very good agreement with those obtained with 3D finite element method. The latter were obtained with a fine mesh discretization of 100 000 hexaedric elements.
- Among the first 20 modes, four special modes appear (see Fig. 5 and Table 4): two torsional modes (1,0,1) and (2,0,1), one axial mode (0,1,1), and one axisymmetric mode (1,0,2). The first three modes do not present any electromechanical coupling due to the radial polarization:

Table 1
Material properties of a transverse isotropic layer and geometrical data of the elastic laminated cylinder [15].

Material properties	Geometric data
E_2=19 GPa, E_1/E_2=2.5	Inner layer thickness =h/3
G_{12}=4.1 GPa	Middle layer thickness =h/3
$\nu_{12} = 0.26$	Outer layer thickness =h/3
$\rho_S = 1643\,\mathrm{kg/m^2}$	h/R=0.002

Table 2
Non-dimensional frequency parameter $\omega^* = \omega R\sqrt{\rho_S/E_2}$ of a [0°,90°,0°] simply-supported laminated cylinder (m=1).

L/R	n	Present	Lam [15]	Zhang [16]
1	1	1.060220	1.061284	1.061283
	2	0.803248	0.804054	0.804052
	3	0.597729	0.598331	0.598328
	4	0.449689	0.450144	0.450140
	5	0.344901	0.345253	0.345248
	6	0.270473	0.270754	0.270747
10	1	0.083825	0.083908	0.083908
	2	0.029978	0.030009	0.030008
	3	0.015176	0.015193	0.015191
	4	0.012161	0.012176	0.012174
	5	0.015214	0.015231	0.015230
	6	0.021156	0.021179	0.021178

Table 3
Frequencies (Hz) of a composite cylinder filled with compressible fluid (m=1).

n	L/R=1		L/R=10	
	Present	FE [17]	Present	FE [17]
1	35.8656	35.8756	2.3887	2.3819
2	30.0713	30.0001	0.9344	0.9336
3	24.4553	24.3251	0.5432	0.5444
4	19.9330	19.7685	0.4902	0.4896
5	16.4431	16.2609	0.6770	0.6703
6	13.7753	13.5850	1.0232	1.0075

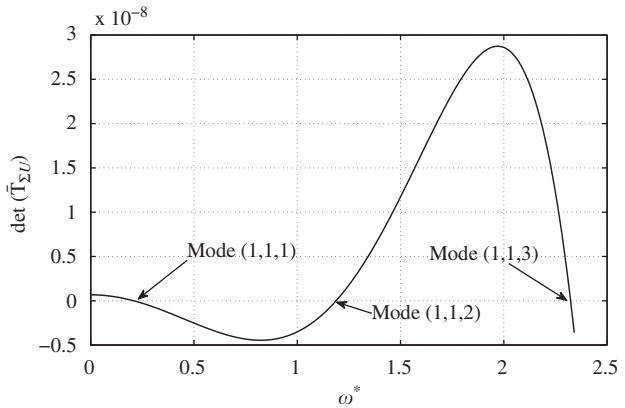

Fig. 3. Solution of the characteristic equation in the elastic case for n=1 and m=1.

- for the two torsional modes (1,0,1) and (2,0,1), we can easily verify from the matrices A_{ij} that there is no coupling between U_θ and Φ if n=0;
- for the axial mode (0,1,1), it clearly appears from the matrices A_{ij} that there is no coupling between U_x and Φ if m=0.

Nevertheless, the electromechanical coupling for the axisymmetric one is important (EMCC >30 percent).

- For the other modes, as expected, the natural frequencies are slightly higher in the open circuited case than in the short circuited case.

For bending mode (1,1,1), through-thickness variations of the mechanical and electrical parameters are now represented and commented.

Figs. 6 and 7 present the thickness distribution of the electric potential and transverse electric displacement. These figures show that the electric potential is almost zero with a quadratic evolution in the SC case and the electric

Table 4
First 20 non-dimensional frequency parameter $\omega^* = \omega R\sqrt{\rho_S/c_{66}}$ of a simply-supported PZT5H cylinder.

No.	(m, n, t)	Elastic Nastran	Elastic exact	Short-circuit	Open-circuit	EMCC (%)
1	(1,2,1)	0.1580	0.1578	0.1845	0.1873	17.09
2	(1,1,1)	0.2079	0.2079	0.2080	0.2219	34.88
3	(2,2,1)	0.3137	0.3136	0.3348	0.3510	30.00
4	(1,3,1)	0.3758	0.3747	0.4537	0.4546	6.40
5	(2,3,1)	0.4264	0.4256	0.5083	0.5119	11.90
6	**(1, 0, 1)**	**0.4711**	**0.4712**	**0.4712**	**0.4712**	**0**
7	(3,2,1)	0.5347	0.5345	0.5566	0.5877	32.07
8	(3,3,1)	0.5350	0.5346	0.6208	0.6313	18.19
9	(2,1,1)	0.5617	0.5617	0.5622	0.5934	32.00
10	(4,3,1)	0.6881	0.6879	0.7808	0.8001	21.84
11	(1,4,1)	0.7022	0.6991	0.8471	0.8496	7.70
12	(2,4,1)	0.7359	0.7333	0.8877	0.8907	8.25
13	**(1, 0, 2)**	**0.7511**	**0.7512**	**0.7512**	**0.7943**	**32.49**
14	(4,2,1)	0.7563	0.7561	0.7849	0.8288	32.10
15	(3,4,1)	0.8014	0.7995	0.9634	0.9683	10.13
16	(5,3,1)	0.8635	0.8635	0.9689	0.9966	23.40
17	(3,1,1)	0.8796	0.8790	0.8811	0.9293	31.77
18	(4,4,1)	0.9020	0.9011	1.0770	1.0856	12.56
19	**(2, 0, 1)**	**0.9420**	**0.9425**	**0.9425**	**0.9425**	**0**
20	**(0, 1, 1)**	**0.9483**	**0.9478**	**0.9478**	**0.9478**	**0**

(i) Elastic case, (ii) short circuited, (iii) open circuited case and (iv) the corresponding EMCC coefficient.

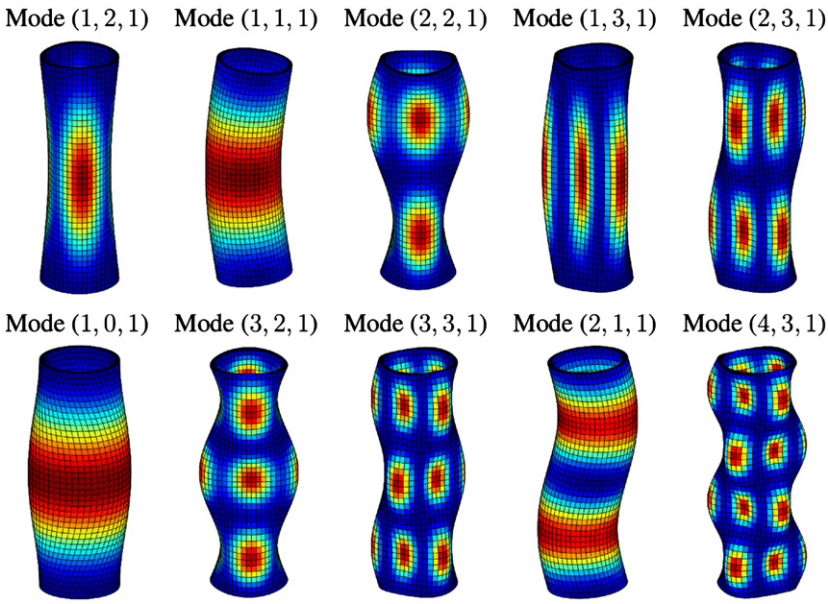

Fig. 4. First 10 modal shapes of a SS piezoelectric cylinder.

displacement is almost zero with a quadratic evolution in the OC case. The results, given by our exact solution, can be used to validate electrical assumptions used in other solutions like finite element method.

Figs. 8 and 9 show the thickness distributions of the mechanical displacements and stresses. As you can see, in contrary of the mechanical stresses that are quadratic, the in-plane mechanical displacements are linear and influenced by the electric boundary conditions. This is due to the fact that this mode is highly coupled (EMCC = 34.88 percent).

Fig. 10 presents the variation of the effective modal EMCC in terms of the half-wavenumbers in the axial and circumferential directions (m and n) for different value of length to thickness ratio (L/H). We can see that the maximum EMCC is always obtained for $m=1$ and $n=1$. For ratio ($L/H=60$), this figure indicates that the effective modal EMCC decreases for the first values of circumferential number n but increases for higher values of n. It indicates also that the EMCC increase slightly with increasing m from $n=4$. The EMCC decreases also with decreasing the length to thickness ratio (L/H).

Table 5 presents the eigenfrequencies of the fluid/piezoelectric–structure coupled system for different electric boundary conditions. As expected, the frequencies are lower in the fluid–structure case due to the added mass effect of the

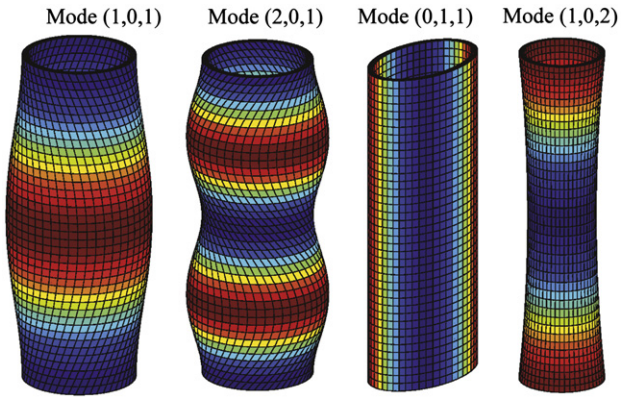

Fig. 5. Special modes: torsional modes (1,0,1) and (2,0,1), axial mode (0,1,1), and axisymmetric mode (1,0,2).

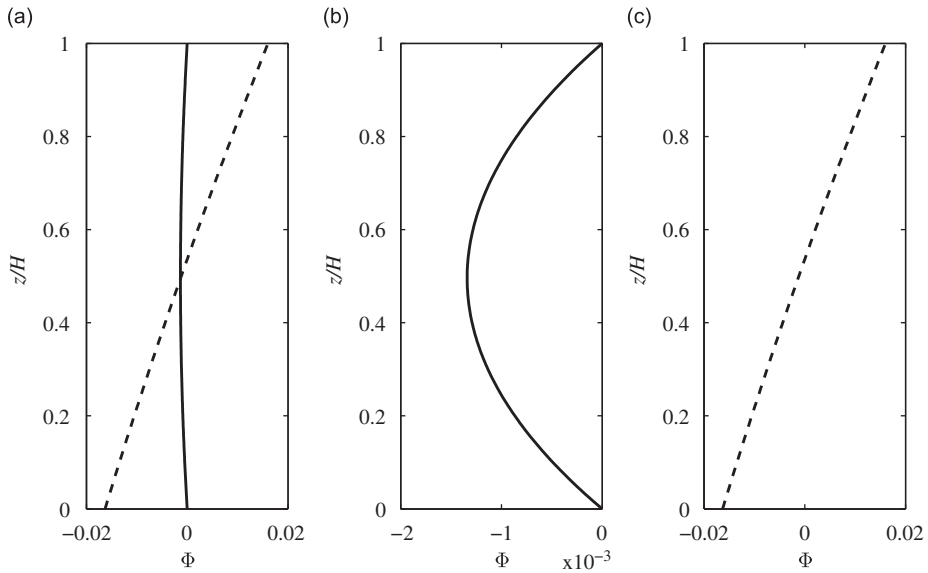

Fig. 6. Through-thickness distribution of the electric potential for the mode (1, 1, 1). SC and OC cases (a), zoom in the SC case (b), zoom in the OC case (c). —— Short-circuited (SC); - - - - open-circuited (OC).

fluid. It is also important to note that the (m,n,t) triplet in the fluid/piezoelectric–structure case is not associated to the same modes as in the case of the piezoelectric–structure in vacuo. In particular, the mode (1,0,2) in Table 5 corresponds to the first fluid mode in rigid cavity. This has been confirmed by comparing the frequency of this mode to the analytical solution given in the book of Blevins [19]. Consequently, this mode does not present any electromechanical coupling. In a same way, the mode (0,1,1) in Table 5 is a pure structural mode. In fact, it corresponds to the axial mode given in Table 4. As discussed previously, this particular mode does not present any electromechanical coupling but also no fluid–structure coupling. This last point can be explained by the fact that the structural displacement is only in the axial direction and therefore not coupled to the fluid which is inviscid.

7.3. Thick laminated piezoelectric cylinder

We consider in this last example a five-layer simply-supported thick cylinder. The geometrical properties of the cylinder are $L=20$ mm, $R=5$ mm and $h=1$ mm. Moreover, the mechanical and material properties of each layer are given in Tables 6 and 7, respectively.

The first 20 modes of the above described simply-supported thick cylinder are calculated using the proposed state-space method in an elastic case (making null the piezoelectric material coefficients of the PZT layers) and in a non-electroded case (considering the electric transverse displacement and potential continuous across the interface between layers so that the piezoelectric layers can be seen as electrically perfectly bonded). In this last case the cylinder top and bottom surfaces are considered free of transverse stresses and electric displacement. Pure elastic modes are also computed

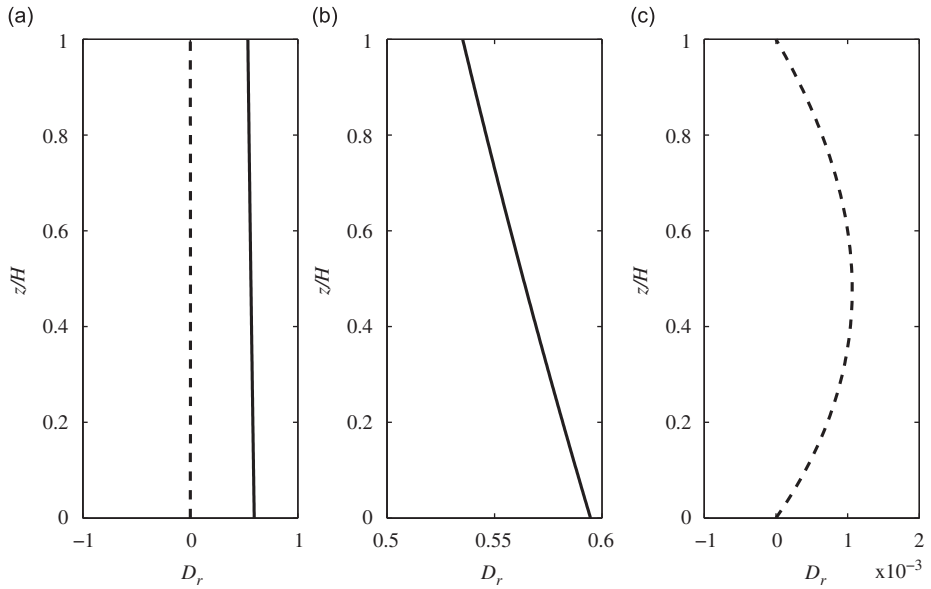

Fig. 7. Through-thickness distribution of the transverse electric displacements for the mode (1, 1, 1). SC and OC cases (a), zoom in the SC case (b), zoom in the OC case. —— Short-circuited (SC); - - - - open-circuited (OC).

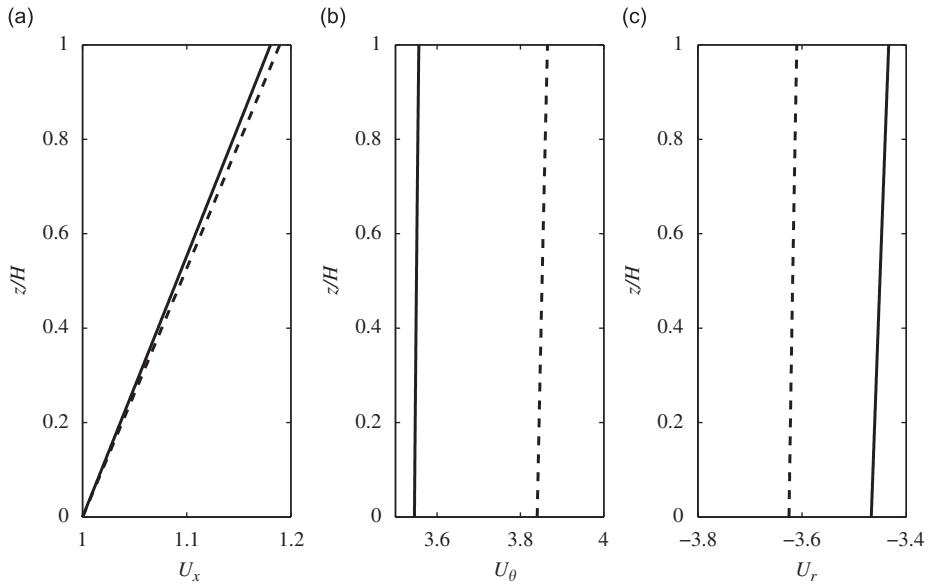

Fig. 8. Through-thickness distribution of the mechanical displacements for the mode (1, 1, 1): axial displacement U_x (a), circumferential displacement U_θ (b), radial displacement U_r (c). —— Short-circuited (SC); - - - - open-circuited (OC).

with the finite element code Nastran. The obtained results are presented in Table 8 for the frequencies and in Fig. 11 for the first four modal shapes for $m=1$.

It can be observed from Table 8 the good agreement between the frequencies obtained with the state-space approach and those obtained from a 3D finite element calculation with a very fine mesh. This comparison validates once again the developed method and provides the modes identification. As shown in Table 8, the elastic frequencies are lower than those calculated in a piezoelectric non-electroded case except for the modes 4, 6, 14 and 20 where the frequencies are exactly the same. These modes correspond to torsion modes (4 and 14) and axial modes (6 and 20) without electromechanical coupling because of the radial polarization of the piezoelectric layers.

Fig. 12 presents the frequency variations with radius-to-length ratio and thickness-to-radius ratio for the first four modes of the simply-supported thick five-layer cylinder. The first graph indicates that the eigenfrequencies increase monotonically with radius-to-length ratio for all modes. Moreover, this increase becomes linear for $R/L \geq 2$. It can be

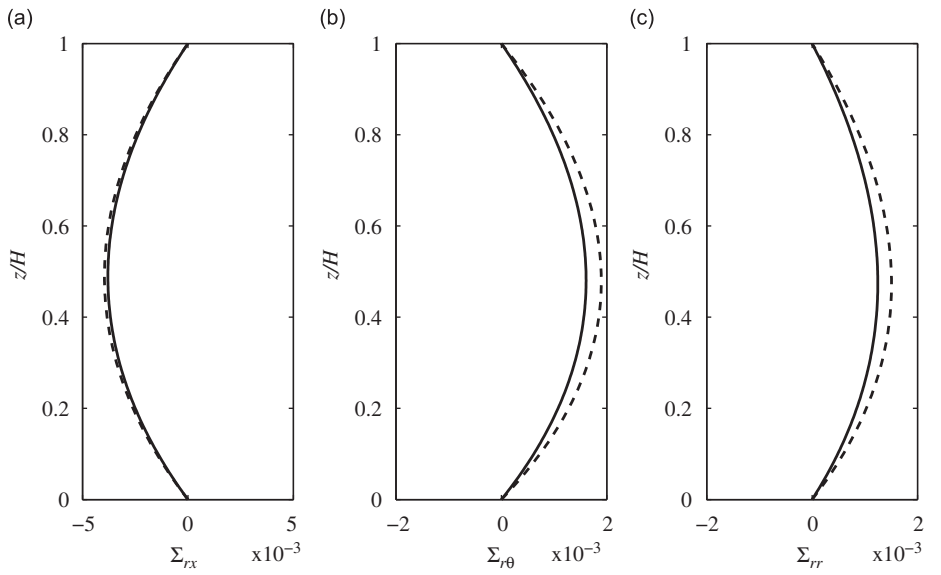

Fig. 9. Through-thickness distribution of the transverse stresses for the mode (1, 1, 1): transverse shear stress Σ_{rx} (a), transverse shear stress $\Sigma_{r\theta}$ (b), transverse normal stress Σ_{rr} (c). —— Short-circuited (SC); - - - - open-circuited (OC).

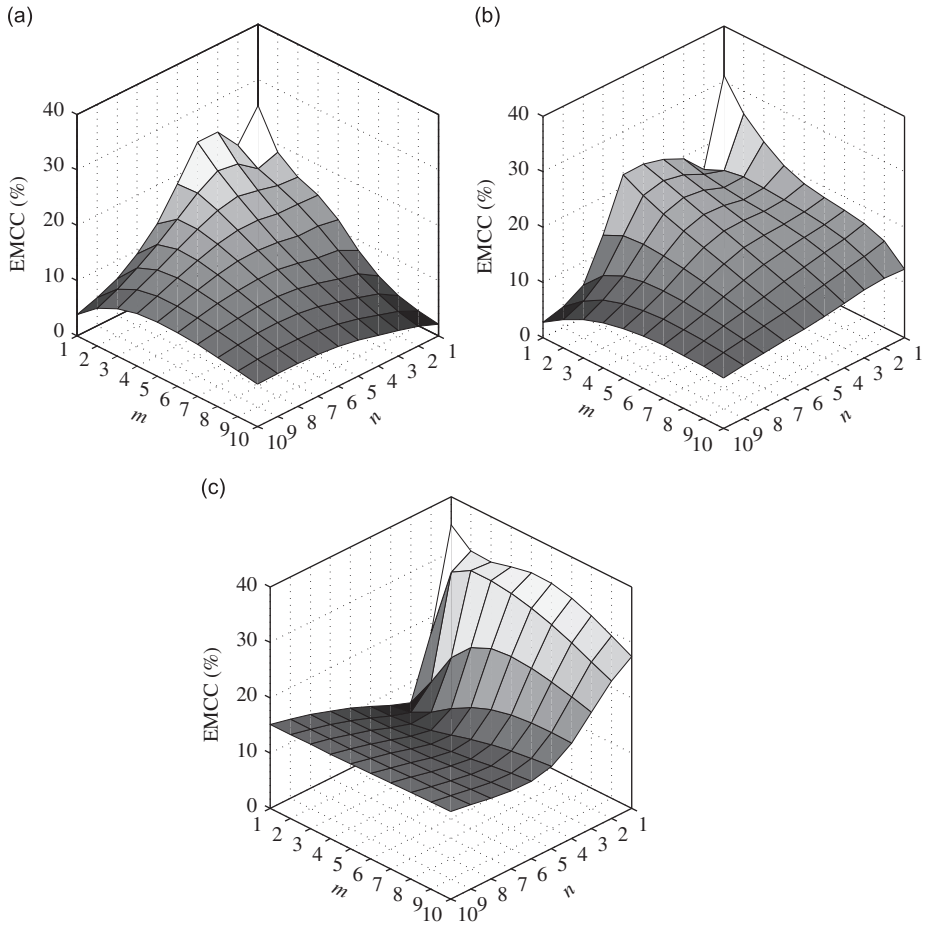

Fig. 10. Variation of the EMCC with m and n for different thickness ratios L/H of a SS piezoelectric cylinder: (a) L/H=5, (b) L/H=10, (c) L/H=60.

Table 5
First 20 non-dimensional frequency parameter $\omega^* = \omega R\sqrt{\rho_S/c_{66}}$ of a simply-supported PZT5H cylinder filled with compressible fluid.

No.	(m, n, t)	Uncoupled	Coupled		
		Elastic	Elastic	Short circuited	Open circuited
1	(1, 2, 1)	0.1578	0.1315	0.1537	0.1562
2	(1, 1, 1)	0.2079	0.1691	0.1692	0.1816
3	(2, 2, 1)	0.3136	0.2634	0.2811	0.2954
4	(1, 3, 1)	0.3747	0.3244	0.3925	0.3934
5	(2, 3, 1)	0.4256	0.3699	0.4414	0.4449
6	(1, 0, 1)	0.4712	0.3006	0.3007	0.3115
7	(3, 2, 1)	0.5345	0.4514	0.4699	0.4979
8	(3, 3, 1)	0.5346	0.4667	0.5415	0.5514
9	(2, 1, 1)	0.5617	0.4545	0.4550	0.4853
10	(4, 3, 1)	0.6879	0.6034	0.6842	0.7024
11	(1, 4, 1)	0.6991	0.6224	0.7531	0.7554
12	(2, 4, 1)	0.7333	0.6540	0.7907	0.7937
13	(1, 0, 2)	0.7512	0.4036	0.4036	0.4036
14	(4, 2, 1)	0.7561	0.6417	0.6658	0.7058
15	(3, 4, 1)	0.7995	0.7150	0.8603	0.8653
16	(5, 3, 1)	0.8635	0.7612	0.8530	0.8792
17	(3, 1, 1)	0.8790	0.6989	0.7005	0.7472
18	(4, 4, 1)	0.9011	0.8084	0.9646	0.9732
19	(2, 0, 1)	0.9425	0.5801	0.5801	0.6044
20	(0, 1, 1)	0.9478	0.9478	0.9478	0.9478

Table 6
Mechanical properties of the laminated piezoelectric cylinder.

Properties	Layer 1	Layer 2	Layer 3	Layer 4	Layer 5
Thickness	$h/5$	$h/5$	$h/5$	$h/5$	$h/5$
Material	PZT-5H	Gr/E 0°	Gr/E 90°	Gr/E 0°	PZT-5H

Table 7
Properties of Graphite-Epoxy and PZT-5H materials.

Properties	Graphite-Epoxy (Gr/E)	PZT-5H
c_{11} (GPa)	183.443	126
c_{22} (GPa)	11.662	126
c_{33} (GPa)	11.662	117
c_{12} (GPa)	4.363	79.5
c_{13} (GPa)	4.363	84.1
c_{23} (GPa)	3.918	84.1
c_{44} (GPa)	2.87	23
c_{55} (GPa)	7.17	23
c_{66} (GPa)	7.17	23.3
e_{15} ($\mathrm{C\,m^{-2}}$)	0	17
e_{24} ($\mathrm{C\,m^{-2}}$)	0	17
e_{31} ($\mathrm{C\,m^{-2}}$)	0	−6.5
e_{32} ($\mathrm{C\,m^{-2}}$)	0	−6.5
e_{33} ($\mathrm{C\,m^{-2}}$)	0	23.3
ϵ_{11} ($10^{-10}\,\mathrm{F\,m^{-1}}$)	153	150.3
ϵ_{22} ($10^{-10}\,\mathrm{F\,m^{-1}}$)	153	150.3
ϵ_{33} ($10^{-10}\,\mathrm{F\,m^{-1}}$)	153	130
ρ_S ($\mathrm{kg\,m^{-3}}$)	1590	7500

observed from the second graph that only two of the four first frequency modes are influenced by the thickness-to-radius ratio, the two others staying constant in terms of h/R.

The exact solution allows the reconstruction of the evolution of the electrical and mechanical quantities through the thickness of the laminated piezoelectric cylinder. These evolutions correspond to variations of the dimensionless quantities U_i, Σ_{ij}, D_i and Φ for $i,j = x,\theta,r$. We present in Figs. 13–15 these evolutions for the first flexion mode (1, 2, 1).

Firstly, we observe that the resulting solution satisfies the boundary conditions imposed on the inner and outer surfaces of the cylinder, i.e. $\Sigma_{rx} = \Sigma_{r\theta} = \Sigma_{rr} = D_r = 0$ for $\bar{r} = 1$ and 1.2. Moreover, we observe from these figures that there is

Table 8
First 25 modal frequencies (kHz) of a simply-supported thick five-layer cylinder.

No.	Mode	Elastic		Non-electroded
	(m, n, t)	Exact	Nastran	Exact
1	(1, 2, 1)	23.290	23.217	25.627
2	(1, 1, 1)	30.014	29.346	30.508
3	(1, 3, 1)	40.674	40.837	45.907
4	(1, 0, 1)	46.174	44.901	46.174
5	(2, 2, 1)	46.531	46.384	49.482
6	(0, 1, 1)	53.575	52.098	53.575
7	(2, 3, 1)	54.763	55.422	60.457
8	(2, 1, 1)	61.715	60.500	63.158
9	(1, 4, 1)	67.206	67.443	74.534
10	(3, 2, 1)	71.555	72.341	75.755
11	(3, 3, 1)	75.236	77.216	81.631
12	(2, 4, 1)	76.810	77.769	84.560
13	(3, 1, 1)	88.632	88.047	91.905
14	(2, 0, 1)	92.342	89.785	92.342
15	(3, 4, 1)	92.676	95.174	100.931
16	(4, 2, 1)	96.978	100.050	102.699
17	(1, 5, 1)	96.984	97.259	105.737
18	(4, 3, 1)	98.701	103.100	106.019
19	(2, 5, 1)	104.459	105.510	113.537
20	(0, 2, 2)	107.115	104.160	107.115

(i) Elastic case (comparison with Nastran) and (ii) non-electroded piezoelectric case.

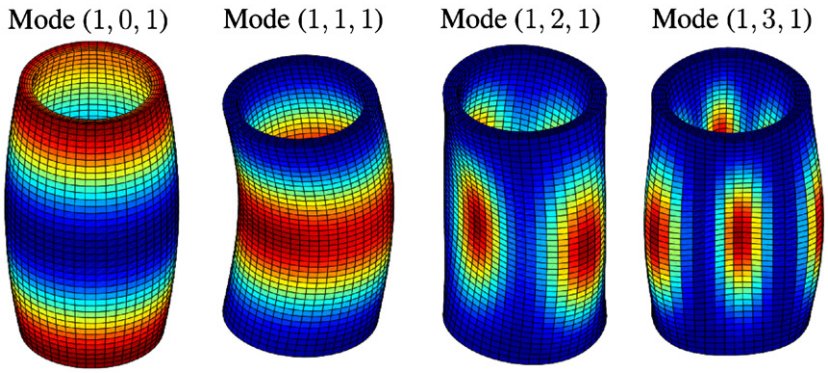

Fig. 11. First four modal shapes for m=1 of a simply-supported thick five-layer cylinder.

continuity of mechanical displacement, transverse stresses, transverse electric displacement and electric potential between the layers. Nevertheless, as the different layers of the laminate cylinder have different composition (different materials or different orthotropy directions), we have discontinuities of the plane stress and the electric displacement components at the interfaces between layers. It should be noted that conditions on $\bar{r} = 1.2$ are not imposed directly, but are found after calculating the reconstitution of all variables by assembling the various sub-layers.

Secondly, the electromechanical coupling of this mode is due to the fact that there is a radial displacement that induces an electric field due to the radial electric polarization.

Finally, our solution being exact, we can accurately plot the evolutions of all parameters in the thickness of the laminated cylinder. For example, since the cylinder is relatively thin (h/R = 0.2), we observe, as expected, that the displacement component U_r is almost constant in the thickness whereas the components U_x and U_θ are quasi-linear.

8. Conclusion

In this paper, an exact 3D mixed state-space solution has been presented for the free-vibration analysis of multilayer piezoelectric hollow cylinders filled with fluid. The piezoelectric layers of the laminated cylinder are supposed to be polarized in the radial direction and the fluid is considered inviscid and compressible. The proposed formulation retains, as state variables, the standard mechanical displacements and transverse stresses augmented with the electric transverse displacement and potential. One of the major advantages of the method is that the resulting eigenvalue problem is only of order four, independently of the number of layers constituting the laminated cylinder. Moreover, the effect of internal fluid

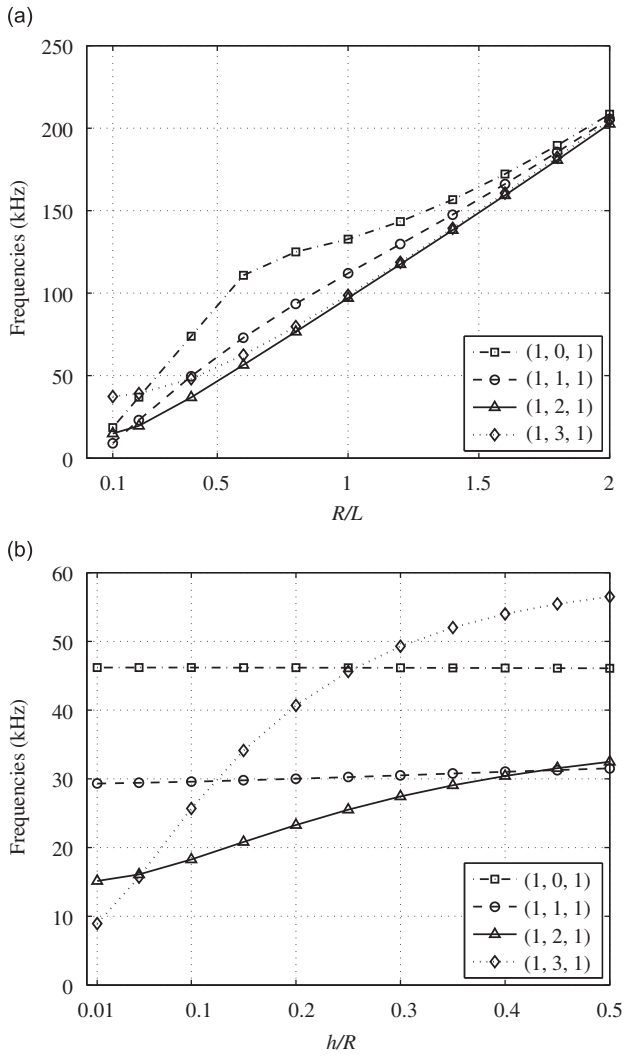

Fig. 12. Frequency variations with radius-to-length ratio (a) and thickness-to-radius ratio (b), for the first four modes of a simply-supported thick five-layer cylinder.

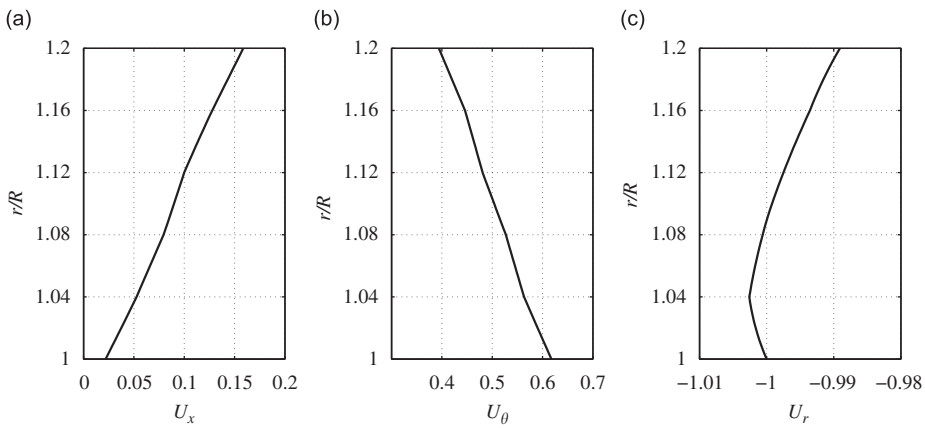

Fig. 13. Mechanical displacements through-thickness distributions for the bending mode (1,2,1) of a simply-supported thick cylinder with non-electroded electric boundary condition: axial displacement U_x (a), circumferential displacement U_θ (b), radial displacement U_r (c).

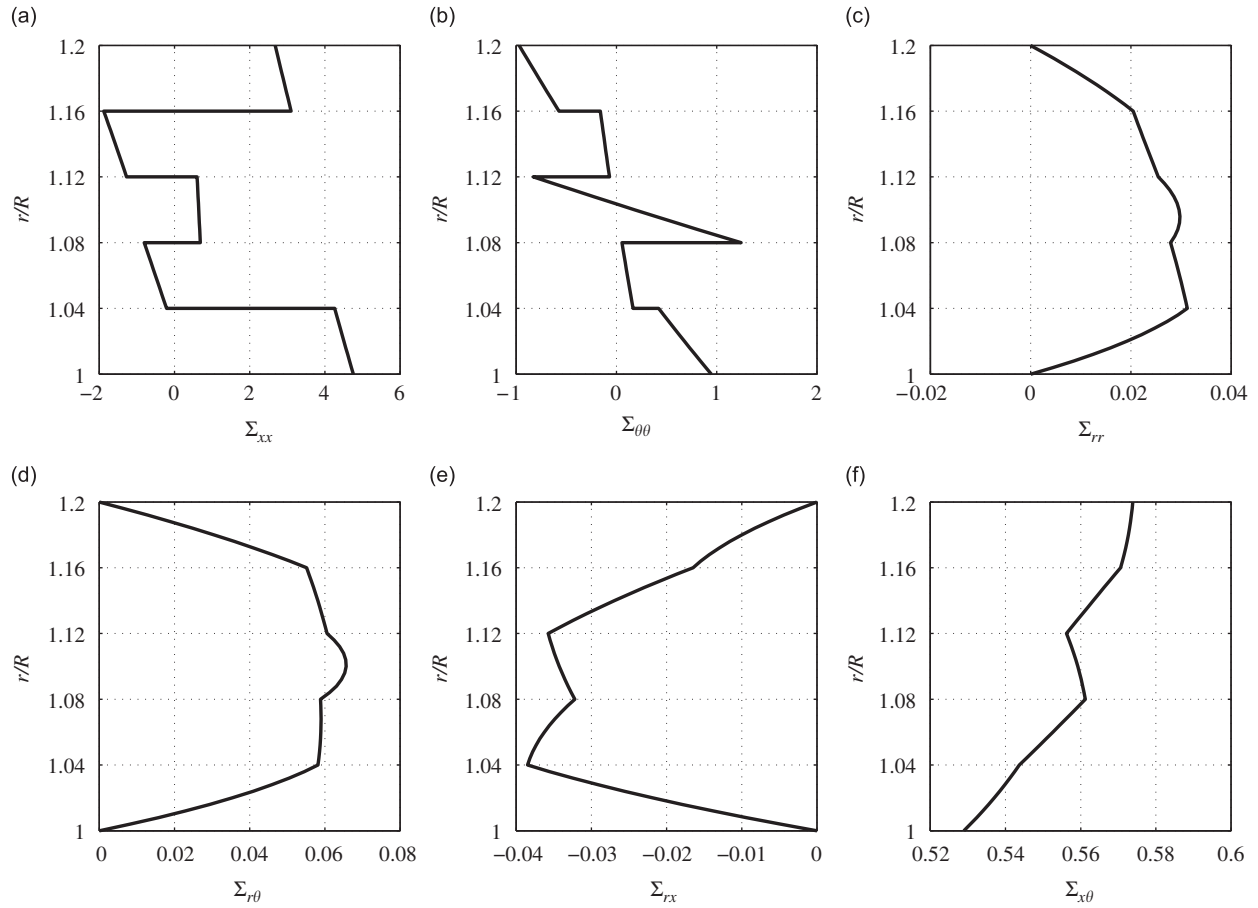

Fig. 14. Mechanical stresses through-thickness distributions for the bending mode (1,2,1) of a simply-supported thick cylinder with non-electroded electric boundary condition: axial stress Σ_{xx} (a), circumferential stress $\Sigma_{\theta\theta}$ (b), radial stress Σ_{rr} (c), transverse shear stress $\Sigma_{r\theta}$ (d), transverse shear stress Σ_{rx} (e), in-plane shear stress $\Sigma_{x\theta}$ (f).

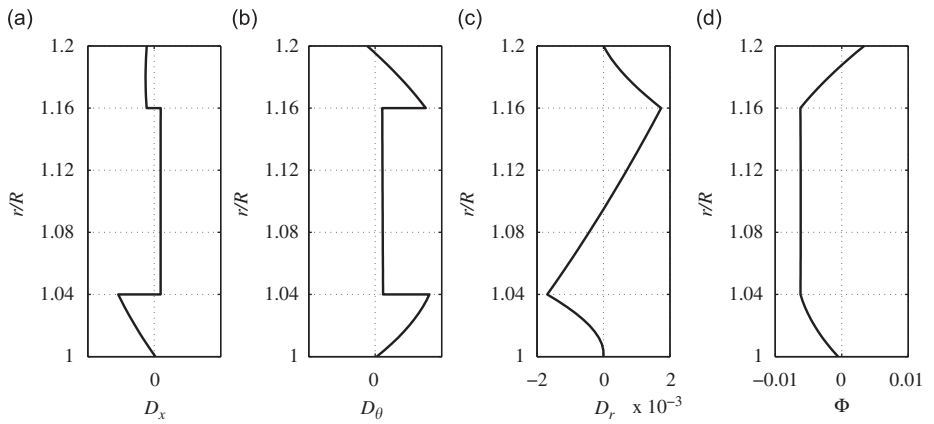

Fig. 15. Electric displacements and potential through-thickness distributions for the bending mode (1,2,1) of a simply-supported thick cylinder with non-electroded electric boundary condition: axial electric displacement D_x (a), circumferential electric displacement D_θ (b), radial electric displacement D_r (c), electric potential Φ (d).

is simply taken into account by imposing a non-zero normal stress at the fluid structure interface. After its validation, the proposed formulation was applied to various examples showing in particular the influence of the electric boundary conditions and of the presence of an internal fluid on the natural frequencies of the coupled system. The results presented

in this paper can be used to clarify the accuracy of approximated shell theories and to investigate the effects of various parameters on the natural frequencies and mode shapes of the fluid–structure coupled system.

Appendix A

Sub-matrices $\mathbf{a}_{ij}$ (for $i,j=1,2$) appearing in Eq. (3):

$$\mathbf{a}_{11}=\left(\begin{array}{c|c|c|c} 0 & 0 & 0 & 0 \\ \hline 0 & \frac{1}{r} & 0 & 0 \\ \hline \frac{c_{12}^*}{r}\frac{\partial}{\partial x} & \frac{c_{22}^*}{r^2}\frac{\partial}{\partial\theta} & \frac{1}{r}\frac{\alpha_{23}-\alpha_{33}}{\alpha_{33}} & \frac{1}{r}\frac{\beta_{23}}{\alpha_{33}} \\ \hline 0 & 0 & 0 & -\frac{1}{r} \end{array}\right)$$

$$\mathbf{a}_{12}=\left(\begin{array}{c|c|c|c} \frac{1}{c_{55}} & 0 & -\frac{\partial}{\partial x} & -\frac{e_{15}}{c_{55}}\frac{\partial}{\partial x} \\ \hline 0 & \frac{1}{c_{44}} & -\frac{1}{r}\frac{\partial}{\partial\theta} & -\frac{1}{r}\frac{e_{24}}{c_{44}}\frac{\partial}{\partial\theta} \\ \hline -\frac{\partial}{\partial x} & -\frac{1}{r}\frac{\partial}{\partial\theta} & \rho_s\frac{\partial^2}{\partial t^2}+\frac{c_{22}^*}{r^2} & 0 \\ \hline -\frac{e_{15}}{c_{55}}\frac{\partial}{\partial x} & -\frac{1}{r}\frac{e_{24}}{c_{44}}\frac{\partial}{\partial\theta} & 0 & \epsilon_{11}^*\frac{\partial^2}{\partial x^2}+\frac{\epsilon_{22}^*}{r^2}\frac{\partial^2}{\partial\theta^2} \end{array}\right)$$

$$\mathbf{a}_{21}=\left(\begin{array}{c|c|c|c} \rho_s\frac{\partial^2}{\partial t^2}-c_{11}^*\frac{\partial^2}{\partial x^2}-\frac{c_{66}}{r^2}\frac{\partial^2}{\partial\theta^2} & -\frac{c_{12}^*+c_{66}}{r}\frac{\partial^2}{\partial x\partial\theta} & -\frac{\alpha_{13}}{\alpha_{33}}\frac{\partial}{\partial x} & -\frac{\beta_{13}}{\alpha_{33}}\frac{\partial}{\partial x} \\ \hline -\frac{c_{12}^*+c_{66}}{r}\frac{\partial^2}{\partial x\partial\theta} & \rho_s\frac{\partial^2}{\partial t^2}-c_{66}\frac{\partial^2}{\partial x^2}-\frac{c_{22}^*}{r^2}\frac{\partial^2}{\partial\theta^2} & -\frac{1}{r}\frac{\alpha_{23}}{\alpha_{33}}\frac{\partial}{\partial\theta} & -\frac{1}{r}\frac{\beta_{23}}{\alpha_{33}}\frac{\partial}{\partial\theta} \\ \hline -\frac{\alpha_{13}}{\alpha_{33}}\frac{\partial}{\partial x} & -\frac{1}{r}\frac{\alpha_{23}}{\alpha_{33}}\frac{\partial}{\partial\theta} & \frac{\epsilon_{33}}{\alpha_{33}} & \frac{e_{33}}{\alpha_{33}} \\ \hline -\frac{\beta_{13}}{\alpha_{33}}\frac{\partial}{\partial x} & -\frac{1}{r}\frac{\beta_{23}}{\alpha_{33}}\frac{\partial}{\partial\theta} & \frac{e_{33}}{\alpha_{33}} & -\frac{c_{33}}{\alpha_{33}} \end{array}\right)$$

$$\mathbf{a}_{22}=\left(\begin{array}{c|c|c|c} -\frac{1}{r} & 0 & -\frac{c_{12}^*}{r}\frac{\partial}{\partial x} & 0 \\ \hline 0 & -\frac{2}{r} & -\frac{c_{22}^*}{r^2}\frac{\partial}{\partial\theta} & 0 \\ \hline 0 & 0 & -\frac{1}{r}\frac{\alpha_{23}}{\alpha_{33}} & 0 \\ \hline 0 & 0 & -\frac{1}{r}\frac{\beta_{23}}{\alpha_{33}} & 0 \end{array}\right)$$

References

[1] P. Heyliger, D.A. Saravanos, Exact free-vibration analysis of laminated plates with embedded piezoelectric layers, *Journal of the Acoustical Society of America* 98 (3) (1995) 1547–1557.

[2] K. Xu, A.K. Noor, Y.Y. Tang, Three-dimensional solutions for free vibrations of initially-stressed thermoelectroelastic multilayered plates, *Computer Methods in Applied Mechanics and Engineering* 141 (1) (1997) 125–139.

[3] A. Benjeddou, J.-F. Deü, Piezoelectric transverse shear actuation and sensing of plates—part 1: a three-dimensional mixed state-space formulation, *Journal of Intelligent Material Systems and Structures* 12 (7) (2001) 435–449.

[4] R.C. Batra, X.Q. Liang, The vibration of a rectangular laminated elastic plate with embedded piezoelectric sensors and actuators, *Computers & Structures* 63 (2) (1997) 203–216.

[5] H.J. Ding, W.Q. Chen, R.Q. Xu, New state space formulations for transversely isotropic piezoelasticity with application, *Mechanics Research Communications* 27 (3) (2000) 319–326.

[6] A. Benjeddou, J.-F. Deü, A two-dimensional closed-form solution for the free-vibrations analysis of piezoelectric sandwich plates, *International Journal of Solids and Structures* 39 (6) (2002) 1463–1486.

[7] J.-F. Deü, A. Benjeddou, Free-vibration analysis of laminated plates with embedded shear-mode piezoceramic layers, *International Journal of Solids and Structures* 42 (7) (2005) 2059–2088.

[8] V.Z. Parton, B.A. Kudryavtsev, *Electromagnetoelasticity: Piezoelectrics and Electrically Conductive Solids*, Gordon and Breach Science Publishers, New York, 1988.

[9] H.S. Tzou, *Piezoelectric Shells: Distributed Sensing and Control of Continua*, Kluwer Academic Publishers, Boston/Dordrecht, 1993.

[10] W.Q. Chen, H.J. Ding, Natural frequencies of fluid-filled transversely isotropic cylindrical shells, *International Journal of Mechanical Sciences* 41 (6) (1999) 677–684.
[11] W. Larbi, J.-F. Deü, Three-dimensional solution for the free vibration analysis of a cylindrical structure with internal liquid, *Proceedings of the First International Congress Design and Modelling of Mechanical Systems*, *CMSM* 2005, Hammamet, Tunisia, March 23–25, 2005 (in French).
[12] W.Q. Chen, Z.G. Bian, C.F. Lv, H.J. Ding, 3D free vibration analysis of a functionally graded piezoelectric hollow cylinder filled with compressible fluid, *International Journal of Solids and Structures* 41 (3) (2004) 947–964.
[13] S.M. Hasheminejad, M. Rajabi, Scattering and active acoustic control from a submerged piezoelectric-coupled orthotropic hollow cylinder, *Journal of Sound and Vibration* 318 (1–2) (2008) 50–73.
[14] J.-F. Deü, W. Larbi, A state space method for free-vibration analysis of a radially polarized laminated piezoelectric cylinder filled with fluid, *Proceedings of the Eighth International Conference on Computational Structures Technology*, *CST* 2006, Las Palmas de Gran Canaria, Spain, September 12–15, 2006.
[15] K.Y. Lam, T. Loy, Analysis of rotating laminated cylindrical shells by different thin shell theories, *Journal of Sound and Vibration* 186 (1) (1995) 23–35.
[16] X.M. Zhang, Vibration analysis of cross-ply laminated composite cylindrical shells using the wave propagation approach, *Applied Acoustics* 62 (11) (2001) 1221–1228.
[17] W. Larbi, J.-F. Deü, R. Ohayon, Vibration of axisymmetric composite piezoelectric shells coupled with internal fluid, *International Journal for Numerical Methods in Engineering* 71 (12) (2007) 1412–1435.
[18] N.N. Rogacheva, *The Theory of Piezoelectric Shells and Plates*, CRC Press, Boca Raton, 1994.
[19] R.D. Blevins, *Formulas for Natural Frequency and Mode Shape*, Krieger Publishing Company, Malabar Florida, 1995.